Available online at www.sciencedirect.com
SCIENCE DIRECT®
Biochemical and Biophysical Research Communications 331 (2005) 1207–1215
BBRC
www.elsevier.com/locate/ybbrc

Crystal structure of human B-type phosphoglycerate mutase bound with citrate ☆

Yanli Wang [a,b], Zhiyi Wei [a,b], Lin Liu [a,b], Zhongjun Cheng [a,b], Yajing Lin [a], Fengyuan Ji [a], Weimin Gong [a,b,*]

[a] National Laboratory of Biomacromolecules, Institute of Biophysics, Chinese Academy of Sciences, Beijing 100101, PR China
[b] School of Life Sciences, University of Science and Technology of China, Hefei, Anhui 230026, PR China

Received 10 March 2005
Available online 19 April 2005

Abstract

The B-type cofactor-dependent phosphoglycerate mutase (dPGM-B) catalyzes the interconversion of 2-phosphoglycerate and 3-phosphoglycerate in glycolysis and gluconeogenesis pathways using 2,3-bisphosphoglycerate as the cofactor. The crystal structures of human dPGM-B bound with citrate were determined in two crystal forms. These structures reveal a dimerization mode conserved in both of dPGM and BPGM (bisphosphoglycerate mutase), based on which a dPGM/BPGM heterodimer structure is proposed. Structural comparison supports that the conformational changes of residues 13–21 and 98–117 determine PGM/BPGM activity differences. The citrate-binding mode suggests a substrate-binding model, consistent with the structure of *Escherichia coli* dPGM/vanadate complex. A chloride ion was found in the center of the dimer, providing explanation for the contribution of chloride ion to dPGM activities. Based on the structural information, the possible reasons for the deficient human dPGM mutations found in some patients are also discussed.

Keywords: Crystal structure; Cofactor-dependent phosphoglycerate mutase; Citrate; Mechanism

Phosphoglycerate mutase (PGM, EC 5.4.2.1) catalyzes the interconversion of 2-phosphoglycerate and 3-phosphoglycerate in glycolysis and gluconeogenesis [1]. There are broadly two classes of PGMs: cofactor-dependent PGM (dPGM) and cofactor-independent PGM (iPGM). The dPGM superfamily contains dPGM, bisphosphoglycerate mutase (BPGM EC 5.4.2.4) [1–3], phosphatase portion of the bifunctional enzyme 6-phosphofructo-2-kinase/fructose-2,6-bisphosphatase (F26Bpase, EC 3.1.3.46) [4], and prostatic acid phosphatase (PAP, EC 3.1.3.2) [5]. Although these enzymes catalyze different reactions, they share a common fold and some conserved residues [6].

Two iso-types of dPGM genes, dPGM-B and dPGM-M, exist in mammals. They can form homodimers MM, BB or heterodimer MB [7]. The B-type dPGM (dPGM-B) is found in brain, liver, kidney, erythrocyte, and early fetal skeletal muscle, whereas the M-type is present in adult skeletal and cardiac muscle [8,9]. The MB heterodimer occurs in heart and in late fetal or neonatal muscle, where the M- and B-types are also both present [7,9].

Besides being involved in the glycolytic pathway, there is increasing evidence that dPGM may regulate the balance between glycolysis and another ATP-producing

☆ *Abbreviations:* PGM, phosphoglycerate mutase; dPGM, 2,3-BPG-dependent PGM; iPGM, cofactor-independent PGM; BPGM, bisphosphoglycerate mutase; dPGM-B, B-type isoenzyme of dPGM; PAP, prostatic acid phosphatase; 1,3-BPG, 1,3-diphosphoglyceric acid; 2,3-BPG, 2,3-diphosphoglyceric acid; Fru26P2ase, fructose-2,6-biphosphatase; 2-PGA, 2-phosphoglyceric acid; 3-PGA, 3-phosphoglyceric acid.

* Corresponding author. Fax: +86 10 64888513.
E-mail address: wgong@sun5.ibp.ac.cn (W. Gong).

0006-291X/$ - see front matter © 2005 Elsevier Inc. All rights reserved.
doi:10.1016/j.bbrc.2005.03.243

pathway, glutaminolysis in tumor cell lines [10]. Recently, it was reported that the expression level of monoubiquitinated dPGM-B is higher in tumor than in the normal tissue [11]. The cellular abundance of the monoubiquitinated dPGM-B tends to increase with the stages of colon cancer, suggesting its correlation with the tumor progression. Thus, the quantification of the ubiquitin-dPGM-B conjugates might have diagnostic or prognostic values.

To deeply understand the catalytic mechanism of human dPGM and its relationship to tumor progression, the detailed structural information is necessary. To date, only the crystal structures of dPGMs from bacteria or yeast such as *Escherichia coli* [12,13], *Saccharomyces cerevisiae* [14–17], *Schizosaccharomyces pombe* [18], *Thermus thermophilus* [19], *Plasmodium falciparum* [19], *Mycobacterium tuberculosis* [19], and *Bacillus stearothermophilus* [20,21] are available. Moreover, the catalytic mechanism of dPGM has not been well defined yet. Previous studies on the substrate binding mode of dPGM showed some contradictory results. Different binding positions of 3-PGA were proposed with the crystal structures of *S. cerevisiae* and *E. coli* dPGMs. Here we report the first crystal structure of human dPGM-B in complex with citrate molecules.

Materials and methods

Crystallization and data collection. The human dPGM-B-$(His)_6$ protein was expressed from pET22b vector in *E. coli* cell and purified by affinity chromatography as described earlier [22]. The optimal crystallization conditions were determined to be 20%(w/v) PEG4000, 18%(v/v) isopropanol, and 0.1 M trisodium citrate dihydrate, pH 5.7, at 277 K. Addition of 0.2 M $(NH_4)_2SO_4$ results in another crystal form with a different space group.

All of the diffraction data were collected at Beijing Synchrotron Radiation Facility (BSRF) equipped with a MAR CCD detector, flash cooled with liquid nitrogen at 100 K. Diffraction data were processed with DENZO and SCALEPACK programs [23].

Structure determination and refinement. Human dPGM-B crystal structures were determined by molecular replacement using AmoRe [24]. The dimer form of *S. cerevisiae* dPGM (Protein Data Bank accession entry 5PGM, Chains A and B) was used as a searching model. Subsequent model building and refinement were carried out with program O [25] and CNS [26]. The improvement of the model was monitored with the help of the R_{free} value. The non-crystallography symmetry restraint was applied during all steps of refinement. Water molecules were included at the later steps of refinement. For each dimer, a strong peak (above 11δ) in the F_o–F_c electron density map was found at the dimer interface. Considering the facts that a chloride ion was found in *E. coli* dPGM crystal structure at the similar position and NaCl is present in the protein solution, this peak was defined as a chloride ion. After refinement, the chloride ion fits the density and the molecular environment very well, with the *B* value at the approximately same level as the residues around. The sequence alignment was carried out using CLUSTAL W [27] and referred to the three-dimensional structural comparison by DALI [28]. The quality and stereochemistry of the final models were analyzed with PROCHECK[29]. Details of data collection and structure refinement statistics are summarized in Table 1.

Table 1
Summary of data collection and structure refinement

	Crystal form I	Crystal form II
Space group	$P2_1$	$P2_1$
Unit cell (Å)	$a = 130.5$	$a = 42.9$
	$b = 75.9$	$b = 65.7$
	$c = 187.0$	$c = 124.8$
	$\beta = 94.4$	$\beta = 94.4$
Resolution limit (Å)	30–2.8 (2.87–2.8)	30–2.7 (2.76–2.7)
Completeness (%)	93.9 (93.8)	94.7 (94.4)
Number of reflections	1,603,227	189,089
Number of independent reflections	85,016	17,981
R_{merge}	0.121 (0.454)	0.129 (0.436)
I/σ	8.6 (2.2)	9.3 (2.3)
R-factor	0.233 (0.340)	0.216 (0.319)
R_{free}	0.272 (0.362)	0.256 (0.372)
Number of non-H atoms		
Protein atoms	22,789	3801
Water molecules	149	120
Citrate molecules	12	2
Chloride	6	1
B-factors (Å^2)		
Main-chain	36.4	30.3
Side-chain	36.2	31.3
Water	23.2	28.0
Chloride	26.4	22.8
r.m.s.d. of bond lengths (Å)	0.007	0.007
r.m.s.d. of bond angles (°)	1.3	1.3

Results and discussion

Structure determination

Two crystal forms of human dPGM-B were obtained. The final model in crystal I contains 12 protein molecules in the asymmetric unit, with *R*-factor of 0.233 and R_{free} of 0.272 at 2.8 Å resolution. The crystal II contains only two protein molecules per asymmetric unit. The final model was refined to 2.7 Å resolution with the *R*-factor and R_{free} of 0.216 and 0.257, respectively. The stereochemistry parameters were proved to be quite good by PROCHECK [29]. The conformations of the total of 14 monomers in two crystals are essentially same, with variations in some loops and the C-terminal regions. Each monomer was found to bind with a citrate molecule. In crystal form II, although ammonium sulfate was added in the crystallization solution, no bound sulfate molecule was found.

The monomer

The fold of the human dPGM-B is quite similar to those of *S. cerevisiae* and *E. coli* dPGMs (Fig. 1). As predicated by the sequence comparison (Fig. 1), the segment from residue 127 to 151, where the sequence homology is low, is structurally different in these three dPGMs. In human dPGM-B, two residues were inserted at residues 136 and 137. This insertion makes an addi-

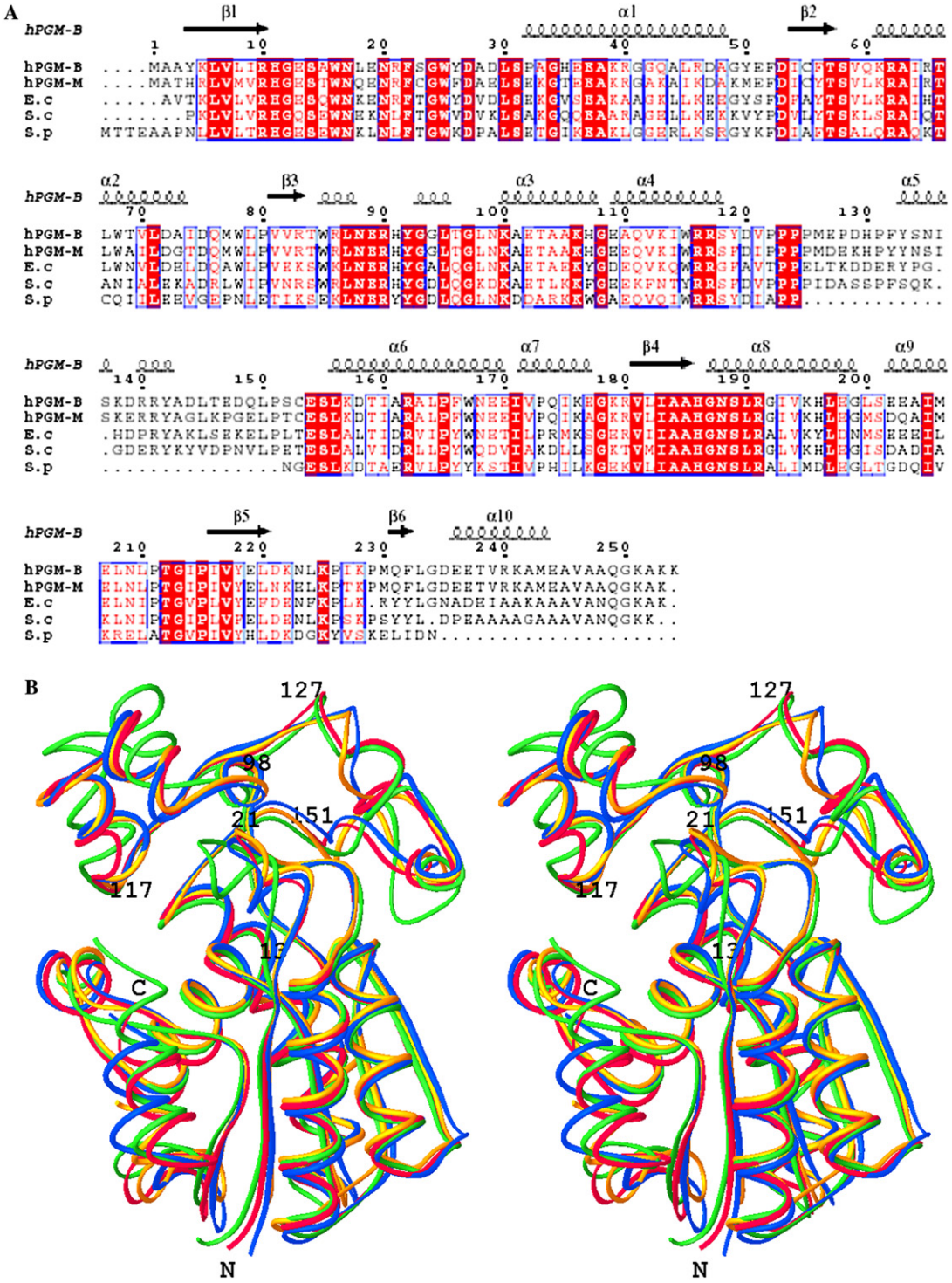

Fig. 1. (A) Structure-based sequence alignment of dPGMs from human type B (hPGM-B), and type M (hPGM-M), *S. cerevisiae* (S.c), *S. pombe* (S.p), and *E. coli* (E.c). The secondary structure elements and residue number of human dPGM-B are shown above the alignment with arrows for β-strands and coils for helices. Strictly conserved and conservatively substituted residues are boxed and marked with red background or colored in red, respectively. (B) Stereo view of the structure comparison of the human dPGM-B (red), human BPGM (green), *S. cerevisiae* dPGM (yellow), and *E. coli* dPGM (blue).

tional short α-helix. Although *E. coli* dPGM has as many residues as that of *S. cerevisiae* dPGM in this region, the conformations are also different between them. In *S. pombe* dPGM, residues 125–152 are absent. Since this region is at the back of the active site, its conformations would be irrelative to the enzyme activities.

Human BPGM shares approximately 50% sequence identity with dPGMs, but has different specific activities.

Compared with dPGMs, the overall fold is similar except residues 13–21, 98–117, 130–150, and the C-terminal tail [30]. The current structure of human dPGM-B indicates that the conformations of residues 130–150 and the C-terminal tail vary in different enzymes, no matter in dPGM or BPGM. However, residues 13–21 and 98–117 keep similar conformations in all of the dPGMs but significantly different from those in BPGM. This further confirms that residues 13–21 and 98–117 would be the structural basis for determining dPGM or BPGM activities.

The homodimer

Human dPGM-B exists as identical homodimers in both of the two crystal forms, dimerized in the same way as *E. coli* dPGM and one dimer of *S. cerevisiae* dPGM. No tetramer as in *S. cerevisiae* dPGM is observed. This suggests that the dimerization mode is conserved during evolution, although the relationship of the dimerization and the activities has not been known. The subunit interactions of human dPGM-B resemble the A–B interface of *S. cerevisiae* dPGM, formed by the anti-parallel alignment of the secondary structures α2 and β3 of the two monomers, with a non-crystallographic 2-fold axis in between. The major contacts are hydrophobic interactions, including Ile64, Trp68, Leu71, Met77, and Val81, especially the side-chain plane of Trp68 stacking to each other. Several charged or polar resides Asp53, Lys61, Arg65, Asp72, Asp75, Gln76, Arg83, and Arg140 are also involved in the dimerization by the hydrogen bonds or electrostatic interactions.

It is worth mentioning that a chloride ion is located near the 2-fold axis of dPGM-B dimer, interacting with the NE1 atoms of Trp68 and the NE2 atoms of Arg83 (Fig. 2), and thus strengthening the interactions of the two monomers. It was reported that low concentration of chloride (5–100 mM) could accelerate the dPGM reaction, while a higher concentration of chloride would inhibit the activity [31]. Based on the structure, chloride ion would help the stabilization of the quaternary structure. However, at higher concentration, the chloride ions could bind at the active site which is rich in positive-charged residues, competing with the substrate and resulting in a lower activity.

The heterodimer

The conserved dimer interface of dPGM is obviously accommodated with the formation of dPGM BM heterodimers. Human dPGM-B dimer is also similar to human BPGM dimer [30]. It has been observed that BPGM can form heterodimers with B-type or M-type dPGM [1,32]. Therefore, in erythrocyte where both dPGM-B and BPGM genes are active, BPGM-dPGM-B heterodimer should be formed by the similar interface. Four of the five residues involved in the hydrophobic dimerization interactions remain the same in human dPGM-B and BPGM (Table 2). The residues contributing to hydrogen bonds or electrostatic interactions vary in dPGM-B and BPGM, resulting in losing some interactions. However, some new interactions in the heterodimer would be formed, including Lys61 of dPGM-B to Glu77 of BPGM, Arg65 of dPGM-B to Glu72 and Glu77 of BPGM, and Glu75 of dPGM-B to His65 of BPGM (Fig. 3). For this reason, the heterodimer should be stable under the physiological conditions.

The flexible gateway for substrates

The active site is located at the bottom of a deep hollow at the C-terminal end of the four-stranded parallel β-sheet. Above the active site, two long loops extend away from the core of the enzyme. The area between these loops leads to a funnel-like active site.

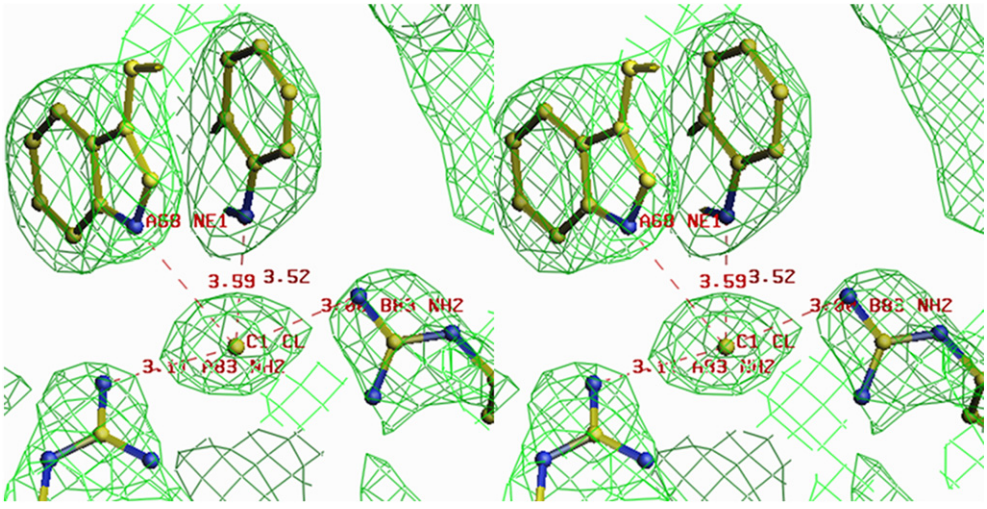

Fig. 2. Stereo view of the interactions between chloride ion and Trp68 and Arg83.

Table 2
The residues whose side-chain is involved in the dimerization interactions in human dPGM-B and BPGM

	Hydrophobic					Polar							
Residue number	64	68	71	77	81	53	61	65	72	75	76	83	140
dPGM-B	I	W	L	M	V	D	K	R	D	D	Q	R	R
BPGM	I	W	L	E	V	D	N	H	E	G	Q	S	R

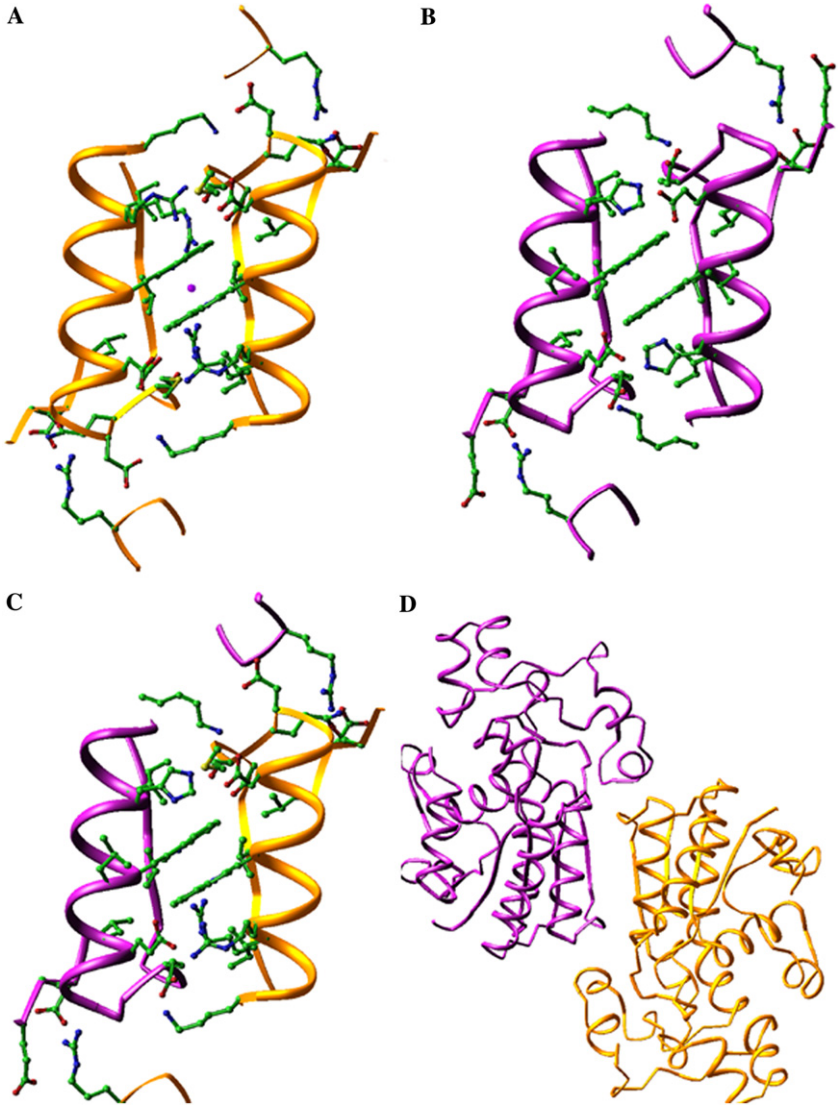

Fig. 3. Dimer interfaces of (A) human dPGM-B, (B) human BPGM, (C) putative human dPGM-B/BPGM, and (D) the dPGM-B/BPGM dimer (dPGM-B, yellow; BPGM, purple).

There are two regions with obviously relatively high *B*-factor values and flexible conformations in human dPGM-B: the C-terminal region which is over the active site and the segment of residue 106–117 which forms one side of the substrate-binding cavity. Some residues (length of 6–13 residues) and the poly-His at the C-terminal tail have no clear electronic density. The *B*-factor values of residue 106–117 in all of the 14 molecules in two crystals are obviously high unless they are involved in crystal packing in some of the molecules, which suggests that this region is likely to be mobile in solution. The disordered C-terminal tail and the high-*B*-valued residues 106–117 have been also observed in other dPGMs and human BPGM structures when no substrate is bound. The flexibility of these two regions may be important in allowing the enzyme to accommodate the entrance of substrate and cofactor.

Active site

His11 is the most important residue by forming a phosphohistidine—the enzyme intermediate as a key

step of the catalytic cycle [33,34]. His11 and most of the residues in the active site are conserved among dPGMs and BPGMs. When superimposing human dPGM-B with other dPGMs, His11, as well as Arg10, Ser14, Thr23, Arg62, Glu89, Arg90, Tyr92, Lys100, Arg116, Arg117, His186, and Asn188 are all fitted very well. This supports that these residues could be involved in the substrate binding or chemical reaction. Two human deficiencies resulted from the mutations of Glu89Ala and Arg90Trp in human dPGM-M [35,36] (which has 81% sequence identity to dPGM-B). Glu89 may act as the acid and base catalyst during the phosphor transfer [16]. Arg90 would bind to the phosphogroup in the substrate (discussed below). Thus, it is reasonable that the substitution of these residues may seriously affect the activity.

p21-activated kinase inhibits glycolysis by association of its catalytic domain with dPGM-B and subsequent phosphorylation of dPGM-B on Ser23 and Ser118 [37]. Ser23 is close to the catalytic residues His11 and Arg62, which may be involved in the proximate phosphogroup binding. Ser118 is next to the basic residues Arg117 and Arg116, which may be involved in the distal phosphobinding. Thereby, their phosphorylation would abolish dPGM-B activity. There would be another reason for decreasing activity by Ser118 phosphorylation. The side-chain of Ser118 is neighboring to the side-chains of Ile114 and Val121. Ser phosphorylation would cause the hydroxyl group of Ser118 to flip from the hydrophobic environment into a hydrophilic pocket and contact with Arg90, Asn188, and Arg191, which might contact the substrates as discussed below.

Another human deficiency has been described related to human dPGM-B isoenzyme with the substitution of Met230 by an Ile. This was thought that the mutation would produce destabilization of the C-terminal helix [38]. In our human dPGM-B structure, Met230 is six residues away from the C-terminal helix thus unlikely to affect its structure. Careful analysis shows that Met23 locates at a strongly hydrophobic area formed by Val194, Leu197, Leu200, Leu208, Leu210 Pro211, Pro226, Pro229, and Phe232, with a charged residue Asp198 close to Met230 at the edge of this area. Asp198 is at the end of helix α8, where it locates the substrate-binding important residues Asn188. Compared to Met, Ile is more hydrophobic. Therefore, this mutation would decrease the structural stability of this area. This is consistent with recent characterization of this deficient mutation [39].

Citrate binding

The active pocket of dPGM is rich in basic residues so that the enzyme can be inhibited by a wide range of anionic compounds in the millimolar to low micromolar concentration range [13,17]. With the carbon backbone similar to that of 3-PGA and partial to that of 2,3-BPG, citrate is a potential inhibitor of dPGM and its binding mode may give a strong evidence for the substrate binding. F_o–F_c electron density shows that a citrate molecule is bound at human dPGM-B active site in both of the two crystal forms. The 14 citrate molecules in two crystals bind at the same position with a similar conformation. The carboxyl group of citrate C1 forms hydrogen bonds with Tyr92 and Arg116. The carboxyl group of citrate C5 interacts with the amide nitrogen of Ser23 and Gly24 (Fig. 4A). The *B*-factors of the citrate molecules are above 60 Å^2 and higher than the surrounding atoms (average *B*-factor of 31 Å^2). Our interpretation is that the citrate does not bind to the protein tightly as the real substrate because its structure is not as favorite as the substrates to the enzyme. However, its binding mode would indicate the general position and orientation of the substrates.

Vanadate, commonly used to study the binding and catalytic mechanism involving phospho- or sulfogroups, was observed to bind with *E. coli* dPGM [13]. Interestingly, the location and orientation of citrate molecule observed here resemble those of the vanadates in *E. coli* dPGM (Fig. 4B). Both of them interact with residues Asn17, Ser23, Gly24, Glu89, Lys100, Arg116, and Asn188 by hydrogen bonds. The two internal vanadates (V2 and V3), with well-defined electron density, locate near the C5 and C1 atoms of the citrate. One oxygen atom of V2 forms hydrogen bonds with the nitrogen atoms of Thr23 (residue in *E. coli* dPGM) and Gly24 similar to citrate C5 carbonyl. The oxygen atoms of V3 form hydrogen bonds with Arg116, Arg117, Arg90, Tyr92, and Asn188, similar to the carboxyl group at citrate C1.

Our observation, as well as the complex structure of *E. coli* dPGM binding with vanadates, strongly suggests that the distal phosphogroup of the substrates would bind at C1 (V3) position, hydrogen bonding to Arg116, Arg117, Tyr92, and Asn188. The carboxyl group of 3-PGA would bind at C5 position and adopt a similar conformation as the C5 carboxyl group of the citrate (Fig. 4C).

The structure of *S. cerevisiae* dPGM provided a different 3-PGA binding mode [40] (Fig. 4D). In that structure, 3-PGA was located with its phosphogroup interacting with Arg62, Thr23, and Ser14, carboxyl group forming a salt bridge with Arg10, and the hydroxyl group at carbon 2 forming a hydrogen bond with the oxygen atom of His11 (human dPGM-B residue number). This binding model is not consistent with our observation. No extra electron density was observed at the corresponding position. Actually the electron density for the 3-PGA was very poor in *S. cerevisiae* dPGM structure. The occupancy for 3PGA was refined to be 0.4. At the same position, a sulfate ion was defined with occupancy of 0.6. Considering the low concentration (1 mM) of 3PGA in the crystallization condition, it is questionable whether the density was interpreted correctly.

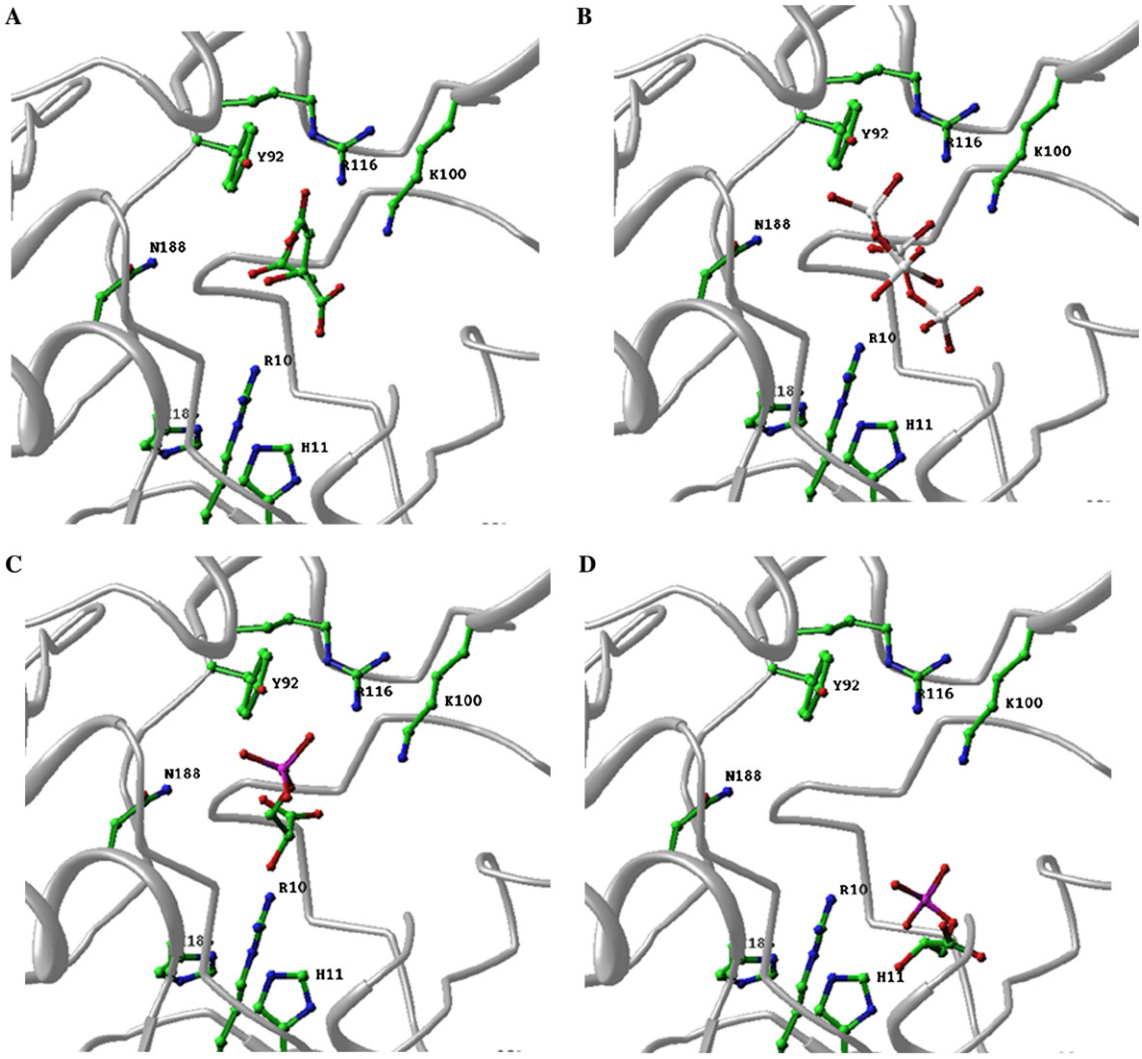

Fig. 4. The comparison of the binding modes of (A) citrate molecule in human dPGM-B, (B) vanadates in *E. coli* dPGM, (C) the proposed 3-PGA, and (D) 3-PGA in *S. cerevisiae* dPGM. The residues of human dPGM-B active site are drawn in ball and stick representation and labeled. Atom coloring: purple, phosphorus; gray, vanadium; green, carbon; red, oxygen; and blue, nitrogen.

In conclusion, the crystal structure of human dPGM-B is reported for the first time. This enzyme remains of a similar fold and the conserved active site as other members in this superfamily. The conformation comparison confirms the conformational differences for dPGM and BPGM specific activities. dPGM-B dimerization interface is same as that of BPGM, suggesting a dPGM/BPGM heterodimer structure. As a general feature of dPGM superfamily, the flexibility of the C-terminus and the segment of 106–117 would be necessary for the substrate entrance. The citrate-binding mode supports the 3-PGA binding model proposed by *E. coli* dPGM/vanadate complex structure.

Protein Data Bank atomic coordinates

Coordinates and structure-factor amplitudes have been deposited with the RCSB Protein Data Bank (PDB) with entrance codes of 1YJX and 1YFK, respectively.

Acknowledgments

This work is supported by the Foundation for Authors of National Excellent Doctoral Dissertation of P.R. China (Project No. 200128), National Foundation of Talent Youth (Grant No. 30225015), The 973 programs (Grant No. 2004CB720000 and No. 2004CB520801) the 863 Special Program of China (Grant No. 2002BA711A13), the Key Important Project and other projects from the National Natural Science Foundation of China (Grant Nos. 10490913, 30121001, and 30130080) and Chinese Academy of Sciences (KSCX2-SW-224). We thank Prof. Peng Liu and Yuhui Dong in Institute of High Energy Physics, and Yi Han in Institute of Biophysics for diffraction data collection.

References

[1] L.A. Fothergill-Gilmore, H.C. Watson, The phosphoglycerate mutases, Adv. Enzymol. Relat. Areas Mol. Biol. 62 (1989) 227–313.

[2] L.F. Hass, W.K. Kappel, K.B. Miller, R.L. Engle, Evidence for structural homology between human red cell phosphoglycerate mutase and 2,3-bisphosphoglysynthase synthase, J. Biol. Chem. 253 (1978) 77–81.

[3] Z.B. Rose, The enzymology of 2,3-bisphosphoglycerate, Adv. Enzymol. Relat. Areas Mol. Biol. 51 (1980) 211–253.

[4] M.O. Lively, M.R. el-Maghrabi, J. Pilkis, G. D'Angelo, A.D. Colosia, J.A. Ciavola, B.A. Fraser, S.J. Pilkis, Complete amino acid sequence of rat liver 6-phosphofructo-2-kinase/fructose-2,6-bisphosphatase, J. Biol. Chem. 263 (1988) 839–849.

[5] G. Schneider, Y. Lindqvist, P. Vihko, Three-dimensional structure of rat acid phosphatase, EMBO J. 12 (1993) 2609–2615.

[6] M.J. Jedrzejas, Structure, function, and evolution of phosphoglycerate mutases: comparison with fructose-2,6-bisphosphatase, acid phosphatase, and alkaline phosphatase, Prog. Biophys. Mol. Biol. 73 (2000) 263–287.

[7] G.S. Omenn, S.C. Cheung, Phosphoglycerate mutase isozyme marker for tissue differentiation in man, Am. J. Hum. Genet. 26 (1974) 393–399.

[8] S.H. Chen, J.E. Anderson, E.R. Giblett, Human red cell 2,3-diphosphoglymutase mutase and monophosphoglyceratemutase: mutase: genetic evidence for two separate loci, Am. J. Hum. Genet. 29 (1977) 405–407.

[9] M.O. Prehu, M.C. Calvin, C. Prehu, R. Rosa, Biochemical and immunological arguments for homology between red cell and liver phosphoglyceromutase isozymes, Biochim. Biophys. Acta 787 (1984) 270–274.

[10] K. Kowanetz, N. Crosetto, K. Haglund, M.H. Schmidt, C.H. Heldin, I. Dikic, Suppressors of T-cell receptor signaling Sts-1 and Sts-2 bind to Cbl and inhibit endocytosis of receptor tyrosine kinases, J. Biol. Chem. 279 (2004) 32786–32795.

[11] T. Usuba, Y. Ishibashi, Y. Okawa, T. Hirakawa, K. Takada, K. Ohkawa, Purification and identification of monoubiquitin-phosphoglycerate mutase B complex from human colorectal cancer tissues, Int. J. Cancer 94 (2001) 662–668.

[12] C.S. Bond, M.F. White, W.N. Hunter, High resolution structure of the phosphohistidine-activated form of *Escherichia coli* cofactor-dependent phosphoglycerate mutase, J. Biol. Chem. 276 (2001) 3247–3253.

[13] C.S. Bond, M.F. White, W.N. Hunter, Mechanistic implications for *Escherichia coli* cofactor-dependent phosphoglycerate mutase based on the high-resolution crystal structure of a vanadate complex, J. Mol. Biol. 316 (2002) 1071–1081.

[14] J.W. Campbell, H.C. Watson, G.I. Hodgson, Structure of yeast phosphoglycerate mutase, Nature 250 (1974) 301–303.

[15] D.J. Rigden, D. Alexeev, S.E. Phillips, L.A. Fothergill-Gilmore, The 2.3 A X-ray crystal structure of *S. cerevisiae* phosphoglycerate mutase, J. Mol. Biol. 276 (1998) 449–459.

[16] D.J. Rigden, R.A. Walter, S.E. Phillips, L.A. Fothergill-Gilmore, Sulphate ions observed in the 2.12 A structure of a new crystal form of *S. cerevisiae* phosphoglycerate mutase provide insights into understanding the catalytic mechanism, J. Mol. Biol. 286 (1999) 1507–1517.

[17] D.J. Rigden, R.A. Walter, S.E. Phillips, L.A. Fothergill-Gilmore, Polyanionic inhibitors of phosphoglycerate mutase: combined structural and biochemical analysis, J. Mol. Biol. 289 (1999) 691–699.

[18] S. Uhrinova, D. Uhrin, J. Nairn, N.C. Price, L.A. Fothergill-Gilmore, P.N. Barlow, Solution structure and dynamics of an open beta-sheet, glycolytic enzyme, monomeric 23.7 kDa phosphoglycerate mutase from *Schizosaccharomyces pombe*, J. Mol. Biol. 306 (2001) 275–290.

[19] H.M. Berman, J. Westbrook, Z. Feng, G. Gilliland, T.N. Bhat, H. Weissig, I.N. Shindyalov, P.E. Bourne, The Protein Data Bank, Nucleic Acids Res. 28 (2000) 235–242.

[20] D.J. Rigden, L.V. Mello, P. Setlow, M.J. Jedrzejas, Structure and mechanism of action of a cofactor-dependent phosphoglycerate mutase homolog from *Bacillus stearothermophilus* with broad specificity phosphatase activity, J. Mol. Biol. 315 (2002) 1129–1143.

[21] D.J. Rigden, J.E. Littlejohn, K. Henderson, M.J. Jedrzejas, Structures of phosphate and trivanadate complexes of *Bacillus stearothermophilus* phosphatase PhoE: structural and functional analysis in the cofactor-dependent phosphoglycerate mutase superfamily, J. Mol. Biol. 325 (2003) 411–420.

[22] Y. Wang, Z. Cheng, L. Liu, Z. Wei, M. Wan, W. Gong, Cloning, purification, crystallization and preliminary crystallographic analysis of human phosphoglycerate mutase, Acta Crystallogr. D 60 (2004) 1893–1894.

[23] Z. Otwinowski, W. Minor, Processing of X-ray diffraction data collected in oscillation mode, Methods Enzymol. 276 (1996) 307–326.

[24] J. Navaza, AMoRe: an automated package for molecular replacement, Acta Crystallogr. A 50 (1994) 157–163.

[25] J. Ta, Z. Jy, C. Sw, Kjeldgaard, Improved methods for building protein models in electron density maps and the location of errors in these models, Acta Crystallogr. A 47 (1991).

[26] A.T. Brunger, P.D. Adams, G.M. Clore, W.L. DeLano, P. Gros, R.W. Grosse-Kunstleve, J.S. Jiang, J. Kuszewski, M. Nilges, N.S. Pannu, R.J. Read, L.M. Rice, T. Simonson, G.L. Warren, Crystallography & NMR system: a new software suite for macromolecular structure determination, Acta Crystallogr. D 54 (Pt 5) (1998) 905–921.

[27] J.D. Thompson, D.G. Higgins, T.J. Gibson, CLUSTAL W: improving the sensitivity of progressive multiple sequence alignment through sequence weighting, position-specific gap penalties and weight matrix choice, Nucleic Acids Res. 22 (1994) 4673–4680.

[28] L. Holm, C. Sander, Protein structure comparison by alignment of distance matrices, J. Mol. Biol. 233 (1993) 123–138.

[29] R.A. Laskowski, M.W. MacArthur, D.S. Moss, M. Valenti, PROCHECK: a program to check the stereochemical quality of protein structures, J. Appl. Crystallogr. 26 (1993) 283–291.

[30] Y. Wang, Z. Wei, Q. Bian, Z. Cheng, M. Wan, L. Liu, W. Gong, Crystal structure of human bisphosphoglycerate mutase, J. Biol. Chem. 279 (2004) 39132–39138.

[31] Z.B. Rose, G.S. Kaklij, The effects of anions on phosphoglycerate mutase, Biochem. Biophys. Res Commun. 121 (1984) 834–841.

[32] R. Rosa, M.C. Calvin, M.O. Prehu, M. Levy-Strauss, J. Rosa, Evidence for the presence of a hybrid of phosphoglyceromutase/bisphosphoglyceromutase in the red cells: partial characterization of the hybrid, Biochem. Biophys. Res. Commun. 120 (1984) 715–720.

[33] C.H. Han, Z.B. Rose, Active site phosphohistidine peptides from red cell bisphosphoglycerate synthase and yeast phosphoglycerate mutase, J. Biol. Chem. 254 (1979) 8836–8840.

[34] Z.B. Rose, The phosphorylation of yeast phosphoglycerate mutase, Arch. Biochem. Biophys. 146 (1971) 359–360.

[35] S. Tsujino, S. Shanske, S. Sakoda, A. Toscano, S. DiMauro, Molecular genetic studies in muscle phosphoglycerate mutase (PGAM-M) deficiency, Muscle Nerve 3 (1995) S50–S53.

[36] A. Toscano, S. Tsujino, G. Vita, S. Shanske, C. Messina, S. Dimauro, Molecular basis of muscle phosphoglycerate mutase (PGAM-M) deficiency in the Italian kindred, Muscle Nerve 19 (1996) 1134–1137.

[37] T. Shalom-Barak, U.G. Knaus, A p21-activated kinase-controlled metabolic switch up-regulates phagocyte NADPH oxidase, J. Biol. Chem. 277 (2002) 40659–40665.

[38] A. Repiso, P. Perez de la Ossa, X. Aviles, B. Oliva, J. Junca, R. Oliva, E. Garcia, J.L. Vives-Corrons, J. Carreras, F. Climent, Red blood cell phosphosphoglycerate mutase. Description of the first human BB isoenzyme mutation, Haematologica 88 (2003) ECR07.
[39] P.d. Atauria, A. Repisoa, B. Olivab, J.L. Vives-Corronsc, F. Climenta, J. Carreras, Characterization of the first described mutation of human red blood cell phosphoglycerate mutase, Biochim. Biophys. Acta (BBA) doi:10.1016/j.bbadis.2004.11.023.
[40] G.S. Crowhurst, A.R. Dalby, M.N. Isupov, J.W. Campbell, J.A. Littlechild, Structure of a phosphoglycerate mutase:3-phosphoglyceric acid complex at 1.7 A, Acta Crystallogr. D 55 (1999) 1822–1826.